Tectonophysics 524–525 (2012) 43–58

Contents lists available at SciVerse ScienceDirect

Tectonophysics

journal homepage: www.elsevier.com/locate/tecto

Combined Seismicity Pattern Analysis, DGPS and PSInSAR studies in the broader area of Cephalonia (Greece)

E. Lagios [a,*], P. Papadimitriou [a], F. Novali [b], V. Sakkas [a], A. Fumagalli [b], K. Vlachou [a], S. Del Conte [b]

[a] Laboratory of Remote Sensing, Department of Geophysics & Geothermics, University of Athens, 157 84 Athens, Greece
[b] Tele-Rilevamento Europa — T.R.E. srl., Via Vittoria Colonna 7, 20149 Milano, Italy

ARTICLE INFO

Article history:
Received 15 July 2011
Received in revised form 8 December 2011
Accepted 10 December 2011
Available online 23 December 2011

Keywords:
Differential GPS
PS Interferometry
Seismicity Pattern Analysis
Cephalonia
Ionian Islands

ABSTRACT

Ground deformation studies based on Differential GPS (DGPS) measurements and Permanent Scatterer Interferometric (PSI) analysis have been conducted on the islands of Cephalonia and Ithaca covering the period 1992 to 2010. DGPS measurements for the period 2001 to 2010 revealed horizontal clockwise rotation of Cephalonia and velocities ranging from 3 to 8 mm/yr with the largest values occurring at the western and southern parts of the island. Considering its vertical deformation, two periods are distinguished on the basis of DGPS and PSI: The first one (1992 to 2003) shows generally an almost linear slight subsidence (around 1 mm/yr) which is consistent with expected neotectonic movements of the island. The second one (2003 to 2010) has been tentatively attributed to dilatancy in which reversal to uplift (2–4 mm/yr) occurred mainly along the southern and southeastern parts of the island, while larger magnitudes (>4 mm/yr) took place at the western part. These non-linear high rates of uplift started at about mid-2005, and were of increasing rate at the southern part, but of decreasing rate at the western part; they may indicate a major regional crustal deformation process in an environment that has previously supported offshore large magnitude earthquakes. Parallel analysis of the observed seismicity in the broader area identified two seismically critical areas on the basis of the decelerating–accelerating seismicity: a major one south of Cephalonia and west of Zakynthos, and another minor one at the NW part of Peloponnese. Critical time estimates of the occurrence of a future strong seismic event in the above critical areas were also made based on: (i) accelerating seismicity, and (ii) the temporal analysis of the seismicity.

1. Introduction

The area of western Greece, and in particular the central Ionian islands, plays an important role in the kinematic processes of the eastern Mediterranean, since it lies within a very active seismotectonically complex area that is undergoing rapid and intense ground deformation. The highest seismic activity in Europe currently takes place in that region, constituting part of the Eastern Mediterranean lithosphere that is subducted beneath the Aegean lithosphere along the Hellenic Arc.

The regional crustal deformation along the entire Ionian Sea and western Greece has been studied through repeat Differential Global Positioning System (DGPS) measurements (e.g. Hollenstein et al., 2008; Reilinger et al., 2010). Also, the additional monitoring of dense GPS networks in the Central Ionian Islands (Zakynthos, Cephalonia, Lefkas) and the broader region of Patras Gulf yielded useful information relating to local ground deformation and kinematics (Lagios et al., 2007; Parcharidis et al., 2009; Vassilakis et al., 2011; Vlachou et al., 2011).

This paper reports on the deformation patterns resulted (i) by recent remeasurements of the GPS network that has been installed in the islands of Cephalonia (2001) and Ithaca (2004) in the central Ionian Sea (Fig. 1) – Lagios et al., 2007 – and (ii) an extensive and thorough Persistent Scatterers Interferometric (PSI) analysis of ERS and ENVISAT radar images of the area, covering the period 1992 to 2008. The regional implications of the PSI and DGPS results are also considered and discussed with respect to the independent outcome of the seismological analysis of the seismicity of the broader area.

2. Brief geological and tectonic setting

The area of western Greece is a case study of interaction between the African and the Eurasian tectonic plates in which the Eastern Mediterranean lithosphere is being subducted beneath the Aegean lithosphere along the Hellenic Arc–Trench System (e.g. Le Pichon et al., 1995). The subduction zone terminates against the Cephalonia Transform Fault (CTF) – Fig. 1 – a major strike–slip fault that links the subduction boundary to the continental collision between the Apulian microplate and the Hellenic foreland (Sachpazi et al., 2000), and plays a key role in the region's geodynamic complexity (Le Pichon et al., 1995; Louvari et al., 1999). Its slip-rate varies from 7

* Corresponding author. Tel.: +30 2107274424; fax: +30 2107274787.
E-mail address: lagios@geol.uoa.gr (E. Lagios).

0040-1951/$ – see front matter © 2011 Elsevier B.V. All rights reserved.
doi:10.1016/j.tecto.2011.12.015

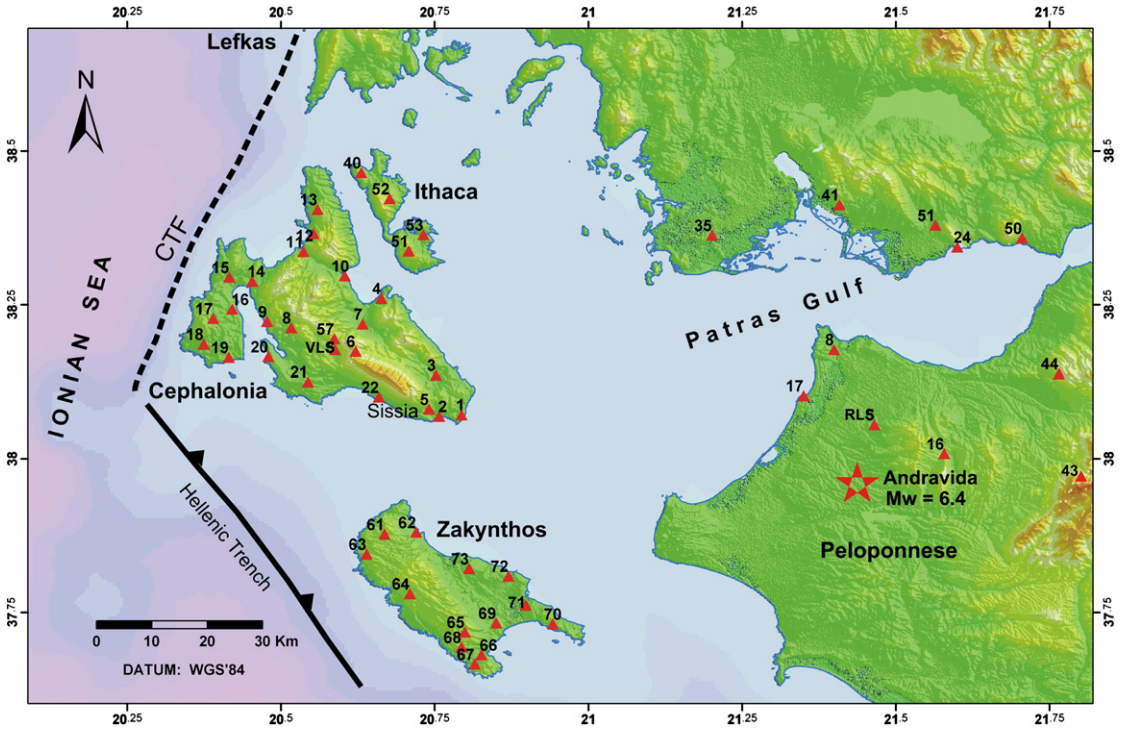

Fig. 1. Broader area of Central Ionian Islands and Patras Gulf indicating the local GPS station networks (CTF: Cephalonia Transform Fault).

to 30 mm/yr based on DGPS measurements (e.g. Anzidei et al., 1996; Hollenstein et al., 2006).

The Ionian zone is dominated by compressional tectonics. The boundary of the zone is defined by the Ionian thrust, which is generally considered to represent the most external structure of the Hellenides. The thrust is well exposed in Cephalonia where a distinct scarp has formed with Mesozoic carbonates of the hanging wall lying next to eroded Miocene marls.

Cephalonia comprises the western part of the fold-belt of the External Hellenides. The island was formed during Tertiary times as a result of the convergence between the African and the Eurasian plates that initiated at the end of the Cretaceous (Kamberis et al., 1996). It mainly consists of Alpine Mesozoic and Cenozoic sedimentary rocks belonging to the External Hellenides, the Paxos or Pre-Apulian zone and the overthrusted Ionian zone (Fig. 2; Aubouin and Dercourt, 1962; Lekkas et al., 2001). The Pre-Apulian zone forms the major part of Cephalonia. The zone has experienced significant late Neogene and Quaternary shortening (Underhill, 1989). The corresponding stratigraphy contains a thick series of Mesozoic to Palaeogene carbonates that are overlain by a series of folded Oligocene to earliest Tortonian deep marine marls and interbedded turbiditic calcareous sandstones (Mercier et al., 1972). Along the southern coast of the island, a series of Messinian clays alternating with mass-transported conglomerate and sand beds emerges beneath a thick series of Messinian evaporites and Lower Pliocene Turbi facies sediments and marls.

The region around Aenos Mt. (see No. 06, in Fig. 1) is dominated by a major asymmetric NW–SE to N–S trending anticline. Further to the east, a zone of intense brecciation occurs bounding these carbonates. Shortening is evident in the western areas of Cephalonia where a series of approximately N–S trending folds and at least one major thrust fault can be traced (Underhill, 1989).

3. Differential GPS measurements

The GPS network in Cephalonia was first installed in 2001 (Fig. 1) and remeasured four times up to early 2006. These data and results have already been presented (Lagios et al., 2007). Another two remeasurements were carried out, one in 2007 (only half of the net was measured) and another one in early 2010. A smaller network was also installed in Ithaca in 2004 (Fig. 1) and remeasured only in 2010, together with the Cephalonia one to study the local ground deformation. All velocity vectors of crustal displacement were calculated and referred to ITRF2000. However, in order to study the local deformation pattern, station velocities were recalculated relative to station No. 06 at Aenos Mt. Therefore, all deformations mentioned in the following figures are referred to the above station. Station No. 06 was chosen as the local GPS reference station, because of its location on the center of the limestone massive Aenos Mt. and its anticipated better geological and tectonic stability compared to other parts of the island. That station was operating continuously during all campaigns.

3.1. Data acquisition

Receivers that were used in all measuring periods were of Leica type, SR399, SR9500 and GRX1200. Each campaign was treated separately. For each daily session, one station was selected as a "connecting station" in the center of the "roving" receiver stations and was tied to the first-order station of No. 06. Each roving station was occupied at least twice with a sampling rate of 15 s, and a nominal duration time of about 10–12 h. Data from a Continuous GPS (CGPS) station at Valsamata (VLSM) recording at 1 Hz since 2005 have also been incorporated in the processing.

3.2. Data processing

The automated processing mode of the Bernese Software v.5.0 (Dach et al., 2007), the Bernese Processing Engine (BPE), was adopted for the long term analysis of the GPS data of the Cephalonia and Ithaca DGPS networks. On a regional scale, horizontal and vertical motion of the broader area of Cephalonia Island was estimated with respect to ITRF2000 using data from the CGPS station VLSM. The use of BPE for data processing of the CGPS station is a necessity given the large amount of daily acquired data. Apart from a time saving technique,

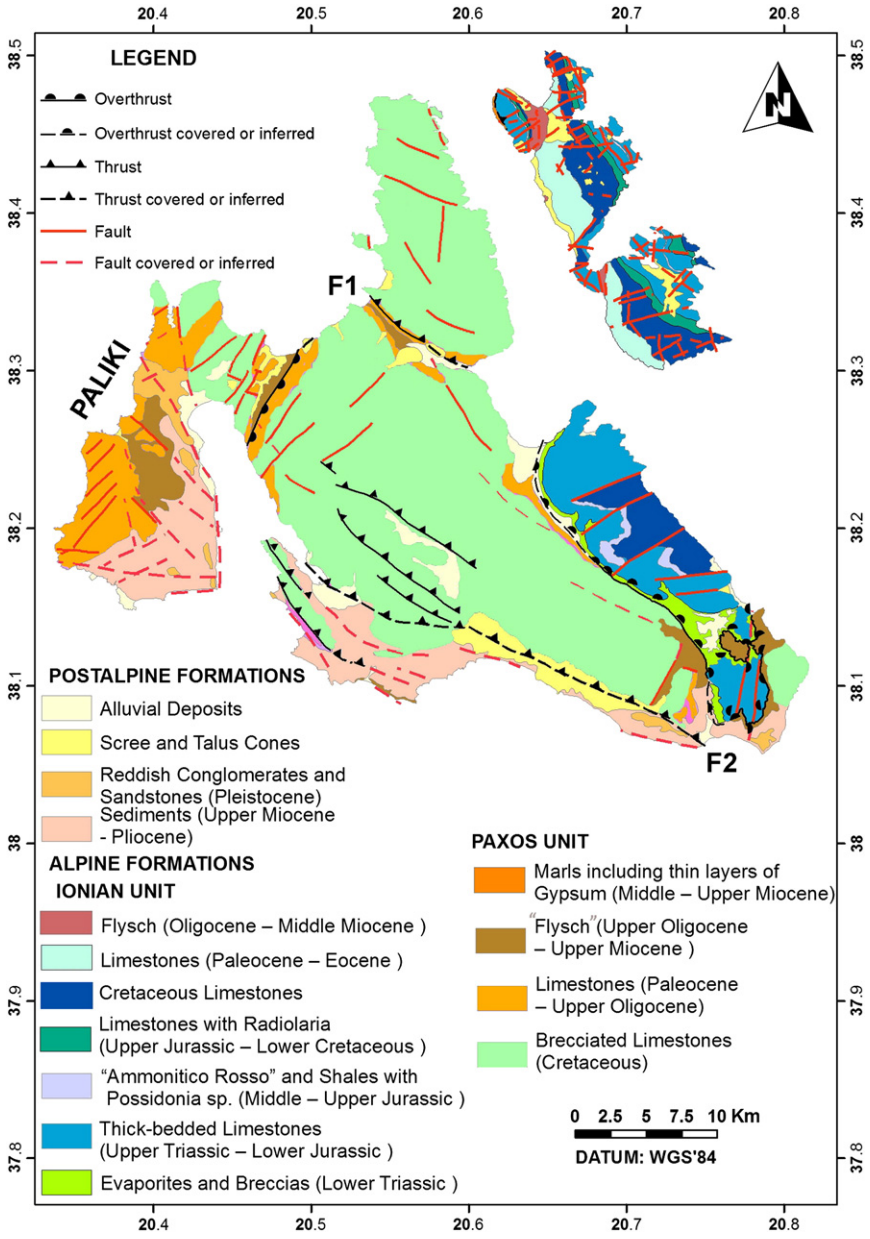

Fig. 2. Geological map of Cephalonia–Ithaca islands. F1, F2: thrusting zones.

the automated mode of Bernese Software offers the unique advantage of Precise Point Positioning (PPP). The PPP was applied on the data of the CGPS station (VLSM) using the observational data from a number of IGS (International GNSS Service) Reference Frame Stations in Europe (http://www.epncb.oma.be/), namely GRAZ (Graz, Austria), MATE (Matera, Italy), SOFI (Sofia, Bulgaria) and WTZR (Bad Kötzting, Germany). Pole, Precise Orbits and Satellite Clock files from the IGS were also used to obtain a set of high precision station coordinates and velocities in ITRF2000.

Analytically, a PPP solution was acquired on a daily basis. The processing procedure included three main parts.

(i) *The Preparatory Part*. Satellite positions from the Precise Orbit files were adjusted to the Bernese extended orbit model (6 osculating elements and 9 dynamical parameters) using associated Pole files. Satellite Clock files were converted to Bernese format.

(ii) *Pre-processing Part*. Pre-processing of the RINEX observation data was accomplished to identify and eliminate cycle slips. Smoothed data were converted into the Bernese format (zero-difference code and phase observation files) and used (code observations only) for the receiver clock synchronization.

(iii) *Processing Part*. Station specific coordinate files were estimated using code and phase measurements. The procedure involved a station by station data reduction with iterative post-fit cleaning. Modelling of the tropospheric delay was done using the Niell Mapping Function — NMF (Niell, 1996) and meteorological data from a standard sea-level atmosphere. A weekly combination of the daily generated PPP files was additionally performed to compute the final coordinate and velocity file associated with the VLSM station. The PPP processing revealed information about the determination of the CGPS station coordinates stability.

The analysis of the local reference station (No. 06) of the DGPS network was also performed using the BPE. Despite the non-continuous operating status of the station, there was an adequate amount of campaign data (8–10 days of continuous recording) for

Table 1
Time series of reference station No. 06 (ITRF2000).

GPS week	Time	E–W	RMS_{E-W}	N–S	RMS_{N-S}	Up	RMS_{Up}
1136	Sep-2001	−77.1	2.3	−17.7	2.6	11.9	4.3
1201	Jan-2003	−53.6	3.2	−5.5	3.5	8.0	4.6
1236	Sep-2003	−47.0	3.1	−11.3	3.6	−5.8	4.3
1364	Mar-2006	0.0	2.8	0.0	3.2	0.0	4.9
1385	Jul-2006	2.7	2.9	−6.2	3.8	−3.7	5.0
1444	Sep-2007	21.5	3.2	2.7	3.5	2.8	5.1
1573	Mar-2010	62.9	3.4	14.3	3.2	5.8	4.0

All values are in mm.

applying the PPP. The station coordinates and velocity were estimated with respect to the IGS reference stations GRAZ, MATE, SOFI and WTZR and were referred to ITRF2000.

The variation of the absolute coordinates (ITRF2000) for station No. 06 is summarized in Table 1 and depicted graphically in Fig. 3, together with the VLSM station. Station No. 06 has a horizontal motion ($V_{East} = 16.5 \pm 0.3$ mm/yr and $V_{North} = 3.3 \pm 0.6$ mm/yr) toward the ENE direction with respect to ITRF2000, while the vertical component seems to be rather stable ($V_{Up} = -0.5 \pm 0.9$ mm/yr). The CGPS VLSM station exhibits similar velocity values as No. 06 ($V_{East} = 17.8 \pm 0.2$ mm/yr, $V_{North} = 3.5 \pm 1.4$ mm/yr and $V_{Up} = 1.3 \pm 1.6$ mm/yr). The overall stability that station No. 06 seems to be exhibiting since 2001 throughout the next 10 years has to be particularly noted, since it represents the local reference point not only for the DGPS analysis, but also for the interferometric analysis that follows in the next section.

The processing procedure applied for the local DGPS benchmark observations was performed using the double-difference based analysis of the automated processing (BPE). The PPP mode was applied as a preparatory BPE processing step, extracting the approximate station coordinates and velocities of the network with respect to IGS reference stations in Europe. The principal steps of the double-difference analysis were the same with the PPP solution (Preparatory and Pre-processing Part). The difference between the two processing strategies (PPP and double-difference) lays in the Processing Part. In the double-difference mode, a data Pre-processing Part was introduced that included the generation of the phase single-difference files, for baseline formation, and the pre-process of the phase single-difference files for cycle slip detection and correction. A double-difference solution was then estimated, generating residuals and normal equation files that were later used for ambiguity resolution. After the observation files were cleaned up from most of the ambiguities, a final network solution was computed resulting in the extraction of the final high precision station coordinates in ITRF2000. Overall rms errors of about 2.0–4.2 mm/yr and 3.7–7.6 mm/yr for the horizontal and vertical components of displacement were respectively achieved for the majority of the stations (at a 90% confidence level). However, there are some stations (Table 2) that exhibit relatively higher errors than the rest of the network. These increased values should rather be attributed to shorter recording time than usually at those stations (e.g. No. 57, No. 12).

3.3. DGPS results

Fig. 4 represents the velocity vectors for three distinct periods of 2001–2003, 2003–2010, and 2001–2010. Table 2 presents the resulting velocity values for the total time period 2001–2010. For the observational period Sept. 2001 to Sept. 2003 small horizontal displacements have occurred (Fig. 4a). The amplitudes were generally less than 5 mm/yr, and only those stations located at the western and northern parts of the island have exhibited values reaching 8–10 mm/yr. The already outlined issue of the clockwise rotation of the island relative to station No. 06 (Lagios et al., 2007) is also observed here. The horizontal velocity vector indicated a southwestward displacement between 3 and 5 mm/yr for stations in the southeastern part of the island, but changing to a northward direction with larger values (≈6 mm/yr) in the central part. Stations located on the Paliki Peninsula at the western part, the horizontal velocity reached values of 8 mm/yr. The northern part of the island appears to have significantly been affected by a major earthquake and its

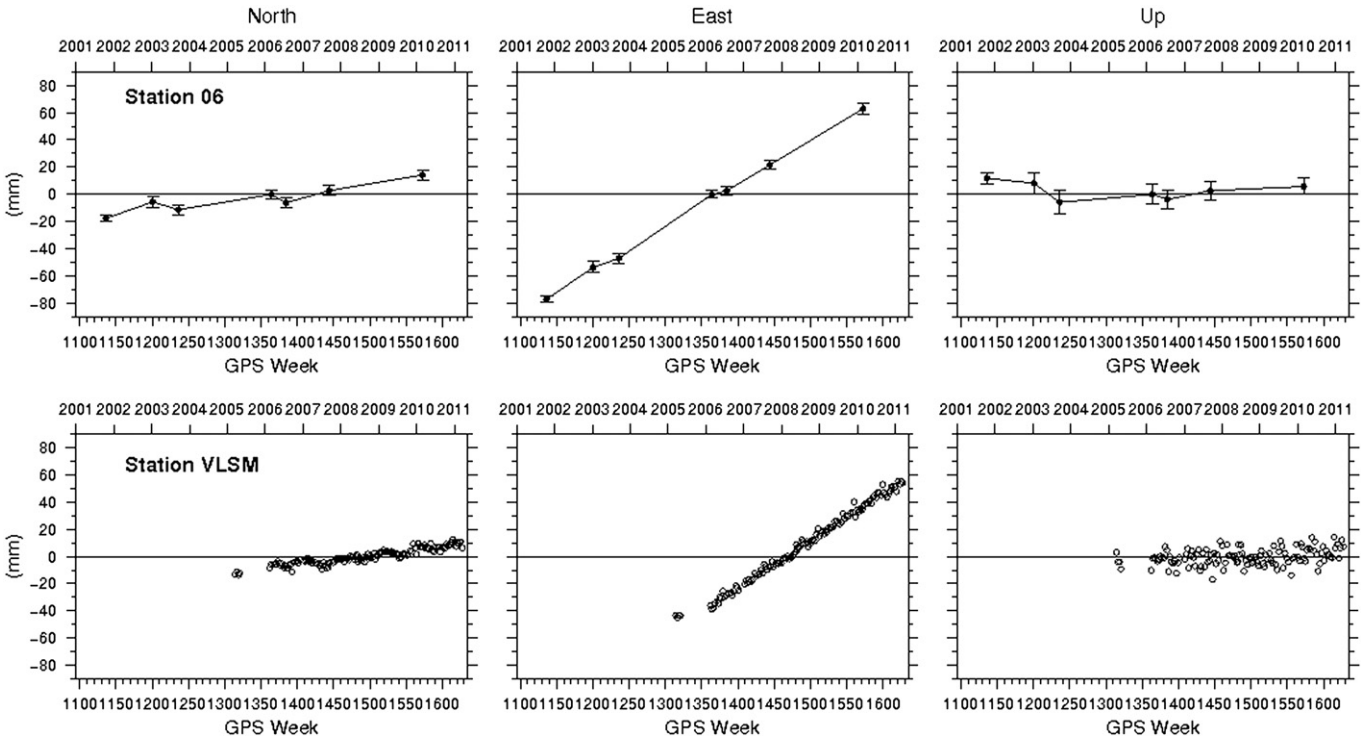

Fig. 3. Component displacements for No. 06 and Valsamata (VLSM) GPS stations with respect to ITRF2000.

Table 2
GPS velocity values (mm/year) referred to No. 06.

Point ID	V_{East}	RMS V_{East}	V_{North}	RMS V_{North}	V_{Up}	RMS V_{Up}
01	−1.4	2.1	−2.7	1.9	−3.3	3.9
02	−1.2	2.2	−1.7	2.0	−0.6	4.1
03	−1.0	2.1	−1.2	1.9	1.4	3.9
04	−1.3	2.8	−1.3	2.5	−0.7	5.2
05	−1.0	2.2	−1.7	2.0	−0.8	4.1
07	−1.2	4.1	1.6	3.7	1.6	7.4
08	1.4	3.1	2.6	2.8	−2.4	5.7
09	2.1	2.5	2.5	2.3	3.1	4.6
10	7.4	2.2	−2.3	2.0	−8.7	4.1
11	0.2	2.8	−0.7	2.5	3.3	5.2
12	3.0	4.2	−0.2	3.8	1.4	7.8
13	1.2	2.0	−1.3	1.8	−3.4	3.7
14	2.5	2.5	1.0	2.3	5.1	4.6
15	2.9	2.1	2.0	1.9	10.0	3.9
16	4.0	2.1	3.2	1.9	6.7	3.9
17	2.4	1.9	5.4	1.7	5.9	3.5
18	3.1	1.9	5.6	1.7	10.8	3.5
19	1.2	3.2	4.6	2.9	5.6	5.9
20	1.0	2.2	2.1	2.0	1.3	4.1
21	2.6	3.8	−0.1	3.4	1.6	7.6
22	−1.3	2.1	1.9	1.9	4.7	3.9
57	0.2	4.1	0.9	3.7	2.9	7.6
40[a]	0.8	2.6	−5.3	2.4	6.0	5.6
51[a]	−2.8	2.6	−3.9	2.4	6.1	5.7
52[a]	−0.8	2.3	−1.7	2.1	4.3	4.5
53[a]	−3.5	2.6	−5.6	2.6	4.9	5.6

[a] Values refer to the period 2004–2010.

post seismic activity that migrated south and offshore, west of the northern Cephalonia, that occurred west of Lefkas Island in August 2003 (Karakostas et al., 2004; Papadimitriou et al., 2006; Zahradník et al., 2005). Note that the horizontal vectors have magnitudes (8–12 mm/yr) that are significantly larger than those in the rest of the island and with direction ESE. Deviations observed at some stations (No. 57, No. 07) from the consistent pattern outlined above should rather be attributed to local phenomena associated possibly with the complex and extensive nature of faulting in the near vicinity.

The vertical component of displacement exhibited behavior that is consistent with the expected tectonic motions of the island. Subsidence that varies from 2 to 10 mm/yr occurred along the southern and south-eastern part. This is a well-known region where systematic neotectonic subsidence is anticipated due to the type of deposits in the area and the associated step-like fault system along the southern part of the Aenos Mt. More intense subsidence (>8 mm/yr) happened at some parts in the western part of the island, in Paliki Peninsula. Small magnitudes of uplift of about 6–10 mm/yr occurred at the central and northern parts of the island, as well as in the eastern part which is characterized by the contact of the Ionian and Paxi tectonic zones. In addition, the presence of evaporites and potentially associated bulging phenomena that may take place there could explain the observed uplift on the east.

For the period 2003–2010 (Fig. 4b), the horizontal velocity vector showed similar behavior with the previous period. The southeastern and western stations seemed to retain their direction and amplitude verifying the clock-wise rotation of the island observed in the first period (2001–2003), while at the central and eastern parts few discrepancies were observed probably due to local tectonism. However, on the northern part, the horizontal vector showed different directions of ground deformation compared to the previous period. The latter may indicate a “rebound” of the whole northern peninsula toward its position prior to the Lefkas earthquake and its post-seismic sequence in August 2003.

Considering the vertical component of displacement, the western part has been uplifted strongly (8–12 mm/yr), while the rest of the island maintained almost a similar behavior as for the period 2001–2003, not showing any distinct change. Specifically, the overall image shows an intense uplift of up to 70 mm at the Paliki Peninsula on the west, with velocities reaching about 13 mm/yr up to 2007, while slight subsidence is subsequently observed from 2007 to 2010, when examining the time series of the GPS stations. At some part of the southern side of the island (Sissia, No. 22, see Fig. 1), smaller values (3–5 mm/yr) of uplift are observed. Strong subsidence, though, has occurred at the northeastern part of the island close to station No. 10, where the subsidence reached 10 mm/yr. However, the subsidence appeared to be almost linear throughout the whole measurement period (2001–2010) in this area, as indicated in Fig. 4c.

The observed deformation for the period 2001 to 2010 presented in Fig. 4c shows that the clockwise rotation of the island with respect to No. 06 still prevailed. The horizontal velocity values range between 3 and 8 mm/yr with the largest ones observed at the Paliki Peninsula. The vertical component indicates that the western part (Paliki Peninsula) has strongly been uplifted at a rate ranging from 5 mm/yr to about 11 mm/yr.

The results associated with the Ithaca Island refer to only one remeasurement period (2004–2010); therefore an inherent uncertainty may be involved due to lack of more remeasurement periods. However, a qualitative image of the island suggests that a differential motion between the northern and southern parts is exhibited, where its southern part has a southwesterly motion with larger velocity values (5–7 mm/yr) than the northern part (2–4 mm/yr). Uplift is generally noticed of about 5 mm/yr. This differentiation in the motion of the northern and southern parts is consistent to the known tectonics of the island, where E–W trending faults divide the island in the middle (Fig. 2). Our observed velocity values at the southern part are consistent to previous GPS work (Hollenstein et al., 2008).

4. Radar interferometry

4.1. The PSInSAR™ technique — basic theoretical concepts

Differential SAR Interferometry (DInSAR) is based on pixel-by-pixel computation of the so-called interferometric phase using two satellite radar acquisitions: such differential phase is a measurement of what has changed in the time interval (35 days for ESA satellites ERS and ENVISAT) between the two images. Apparent phase variations between two satellite scenes can be caused by actual ground displacement or by atmospheric effects that delay electromagnetic wave propagation. The PSInSAR™ technique (i.e. Ferretti et al., 2000, 2001; Heleno et al., 2011) allows atmospheric effect to be estimated and then removed by combining data from long time series of SAR images (such as those available in the ESA-ERS archive) which were acquired from late 1991.

The approach is based on a few basic observations: atmospheric artifacts show strong spatial correlation within individual SAR acquisitions but are uncorrelated in time and, conversely, target motion is usually strongly correlated in time, exhibiting varying degrees of spatial correlation depending on the type of deformation (e.g. subsidence due to water pumping, fault displacements, localized sliding areas, collapsing buildings, etc.). In order to improve the accuracy of ground displacement estimations, only scatterers minimally affected by temporal and geometrical decorrelations are selected for processing (Ferretti et al., 2000, 2001). Differential phase contributions generated by atmospheric effects can be separated from stable ground signals (known as Permanent Scatterers, or PS) if the temporal span of SAR data used is wide enough (typically about 30 images). Given the high spatial correlation of the Atmospheric Phase Screen (APS), even a sparsely populated grid of measurements allows a reasonable sampling of atmospheric phase contributions, provided a PS density of at least 3–4 PS/km^2.

After the removal of the APS, sub-meter elevation accuracy is achievable and millimetric terrain displacements can be detected through the exploitation of extensive temporal satellite data archives.

In particular, target velocity in the line of sight (LOS) of the satellite can be estimated with accuracy often greater than 1 mm/year, allowing accurate verification of deformation models, a key issue for risk assessment. Results of multi-interferogram analysis are mapped with individual time-series data and LOS velocities available for each PS (typical coordinate system used is WGS'84). Common to all differential interferometry applications, the results are computed with respect to a GCP of known elevation and motion. Based on the

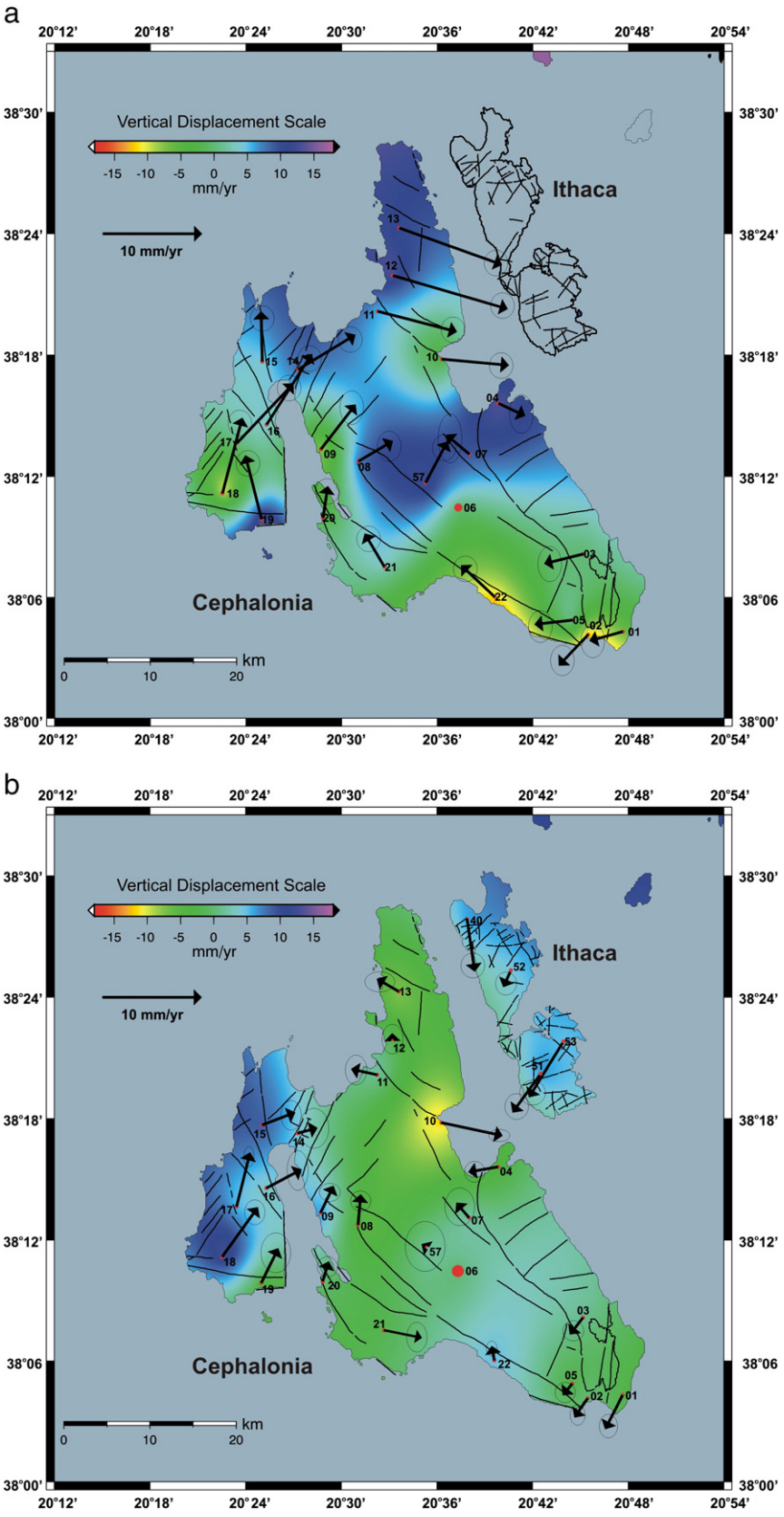

Fig. 4. Vertical and horizontal velocity map for the period 2001–2003 (a), 2003–2010 (b), and 2001–2010 (c).

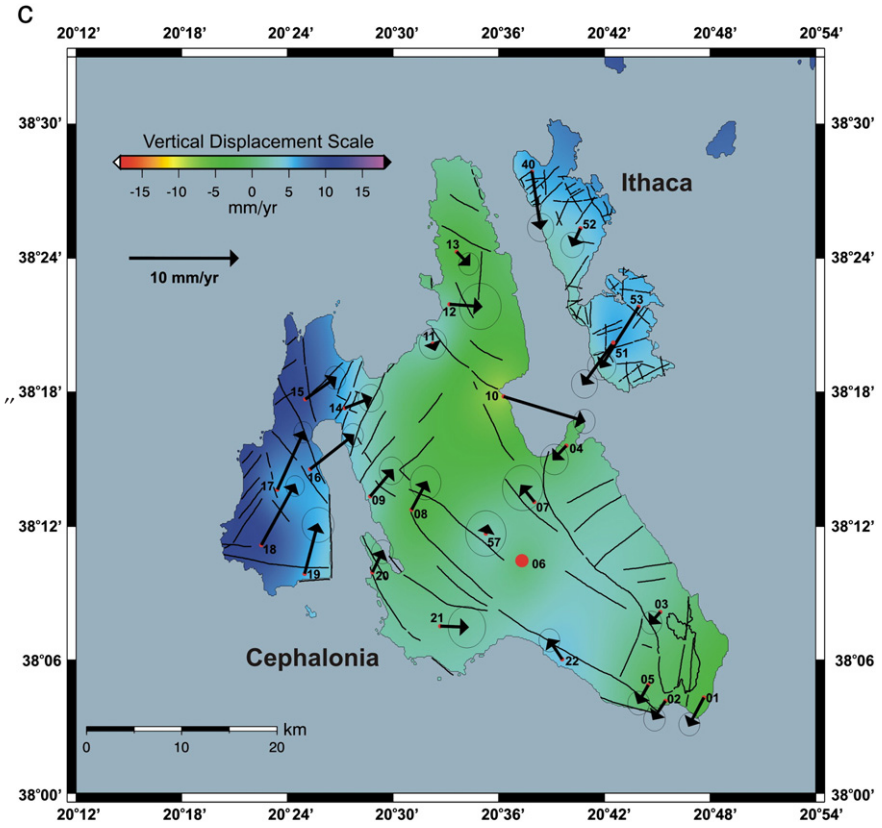

Fig. 4 (*continued*).

orbital satellite geometry (see insert in Figs. 5 and 6), it is evident that the vertical velocity deformation of a PS point is 0.923 of the LOS velocity. Therefore, since the LOS velocity of a PS point may be considered as describing its vertical motion at a close approximation (≈92%), the term vertical deformation (uplift or subsidence) is adopted hereafter to describe the velocity direction of the PS points.

4.2. Application of PSInSAR™ technique

Sixty seven SAR scenes acquired by ERS-1 and ERS-2 satellites were processed, covering the period April 1992 to December 2000. More than 800,000 PS points in descending geometry were identified within an areal extent of about 1400 km^2. Fig. 5 shows the PS product of the velocity deformation field (in mm/yr), covering the period April 1992 to December 2000, resulting from the analysis of 39 descending radar images (Table 3). In addition to the ERS archive, 21 ENVISAT descending scenes acquired on the same area for the period June 2003 to November 2008 (Table 3) were processed, resulting in more than 600,000 identified PS points (see Fig. 6).

The GPS reference base station at Aenos Mt. (No. 06) was chosen as a common ground control point (GCP) for all subsequent differential interferometric analysis. This is a point of a proved stability since at least 2001 (Fig. 3) that also provides a direct comparison between the produced PS image and the DGPS results.

4.3. The velocity field

The PS image of the velocity field from the ERS descending data covered the period 1992–2000 (Fig. 5). It has generally shown a motion being consistent with the vertical movements anticipated by the known tectonism of the area. The northern part, above the thrust zone F1 showed a small uplift (<1.5 mm/yr) with small patches of subsidence, mainly controlled by the local faulting features. The western part of Cephalonia along the Paliki Peninsula exhibited a similar deformation pattern, but with a higher subsidence rate (−2.3 mm/yr), especially along the western coastal zone. However, the lack of coherence in the largest part of Paliki Peninsula does not allow any sufficient outline of deformation estimates. A coherence threshold of 0.62 for the ERS and 0.74 for ENVISAT data sets has been set for the selected PS points to have a reliable velocity value. In the central and southeastern parts of Cephalonia, the observed deformational pattern is mainly controlled by the major thrusting zone F2 that runs along the SE side of the island. Small uplift rates of about 1 mm/yr and significant subsidence rates of up to −2.3 mm/yr were deduced across that zone. A similar pattern to the Cephalonian image was also observed in Ithaca where the largest part of the island presented a slight uplift (≈1.5 mm/yr), while small parts of coastal areas on the west and SE have subsided with rates of −2 mm/yr (Fig. 5).

The PS image from the ENVISAT data covering the subsequent period of 2003 to 2008 was significantly different (Fig. 6). The difference was especially profound along the F2 thrusting zone and the Paliki Peninsula (Fig. 5), where subsidence or slight uplift rates changed to significant uplift rates up to 4 mm/yr (Fig. 6). At Paliki Peninsula, the sign of the vertical component of deformation reached strong uplift rates (>3 mm/yr) at its northwestern part, but with smaller rates on its southern part (≈1 mm/yr). Strong uplift rates were also observed along both sites of the F2 trusting zone; there have been areas along that zone where the change of the vertical velocity reached uplifting values up to 6 mm/yr. At the northern peninsula of the island, the generally slight uplift that has been observed for the period 1992 to 2000 (ERS data) changed to strong uplift (>3 mm/year) in the extreme northern part, while strong subsidence (<−2 mm/year) was noticed just north of the F1 thrusting zone that seems to largely control the deformation pattern across that feature. The eastern part of the island was the only area where the

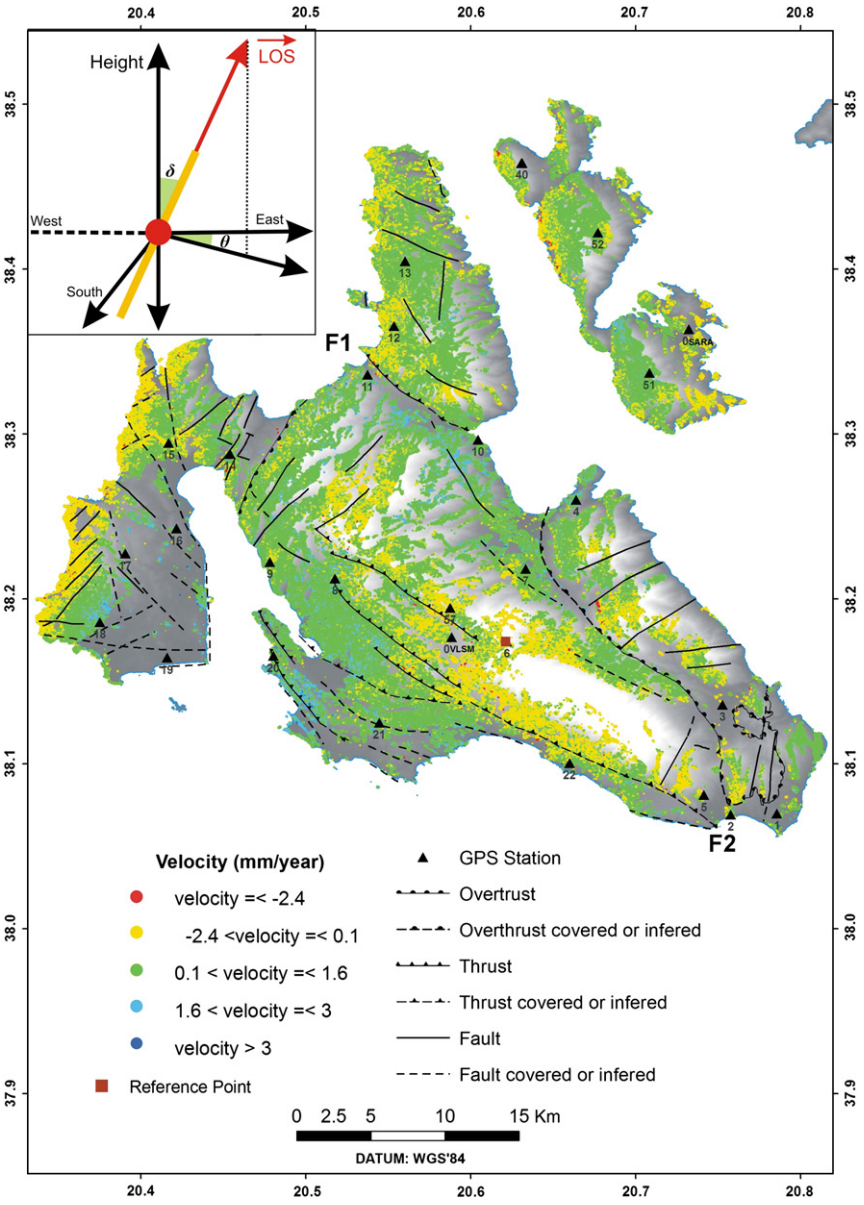

Fig. 5. PSInSAR™ velocity deformation map deduced from ERS descending radar imaging (1992–2000). The inset figure describes the orbital satellite geometry of line of sight (LOS) direction. For ERS satellites LOS versor coordinates are: N = −0.082, E = 0.374 and H = 0.924; LOS angles are: $\theta = 12.4°$ and $\delta = 22.52°$.

deformation showed an almost constant pattern during both periods of our ERS and ENVISAT data, where rather insignificant patches of small subsidence or uplift rates were marked.

Ithaca Island appeared to retain the overall tendency for uplift, but its rate was increased (>2.5 mm/year) during the ENVISAT observational period. The steep slopes on the west are the only parts of the island that subsided, but they should rather be attributed to slow landslide associated phenomena probably taking place along these coastal areas.

4.4. The standard deviation

The standard deviation of the velocity field was also computed for both ERS (Fig. 7) and ENVISAT (Fig. 8) data. There are two parameters affecting the calculation of the standard deviation:

(i) *The deviation of motion from the linear model.* Since the standard deviation is associated with the average rate of deformation, a PS point that exhibits a strong non-linear motion would result in a large residual with respect to the linear model, and thus in a high standard deviation value. This, therefore, allows identifying areas being affected by motion-dynamics that are more complex than the linear model, and in any case it shows a clear deviation from a linear velocity pattern of ground deformation.

(ii) *The distance of each PS point from the reference point.* The displacement model is estimated on the phase-difference between the point under analysis and the reference point, in order to mitigate the effect of the atmospheric noise, which is strongly spatially correlated. However, moving away from the reference point, the difference between its atmospheric contribution and the atmospheric contribution of the PS point under analysis tends to increase producing a larger residual after the estimation of the linear model. The latter is represented by the standard deviation of the corresponding estimated average velocity. Therefore, the velocity standard deviation increases moving away from the reference point.

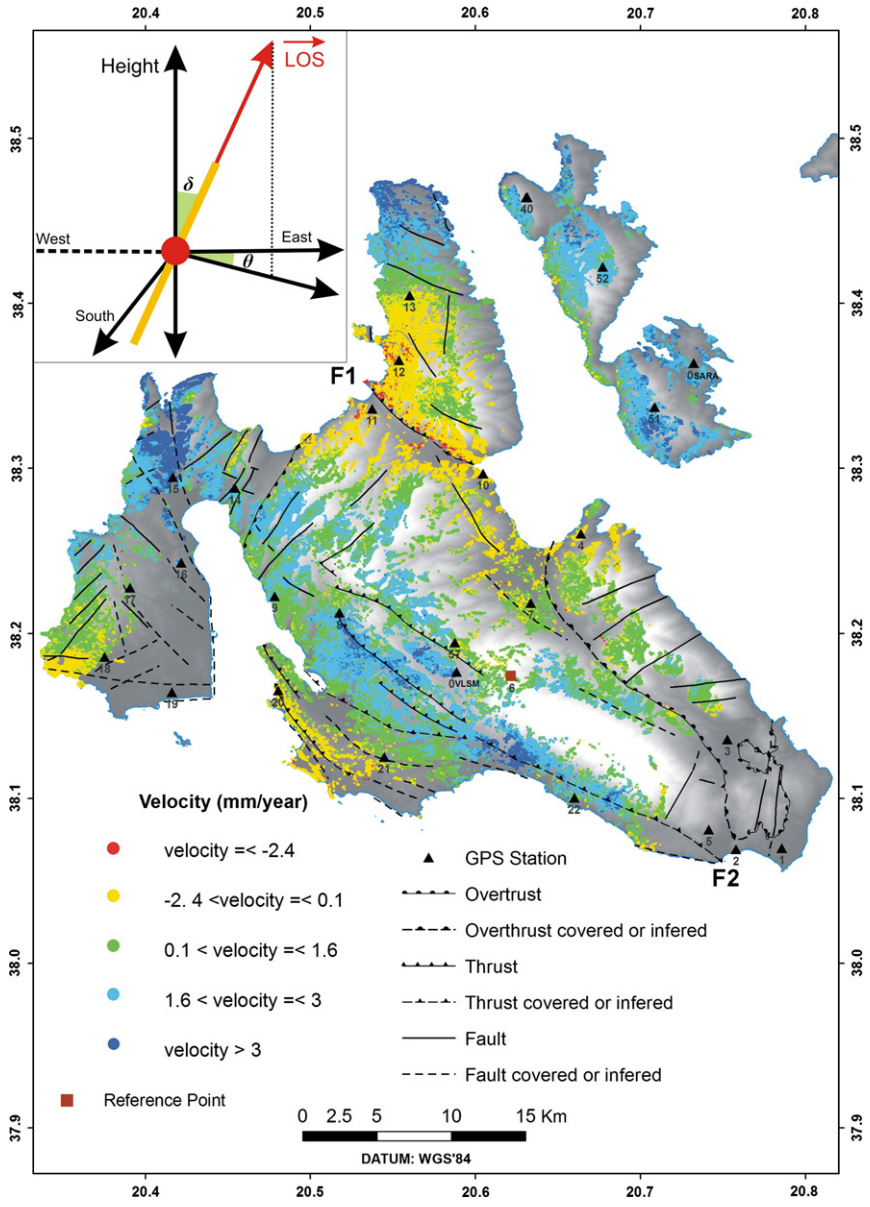

Fig. 6. PSInSAR™ velocity deformation map deduced from ENVISAT descending radar imaging (2003–2008). The inset figure describes the satellite orbital geometry of line of sight (LOS) direction. For ENVISAT satellite versor coordinates are: N = −0.083, E = 0.376 and H = 0.923; LOS angles are: $\theta = 12.4°$ and $\delta = 22.66°$.

The standard deviation of the ERS velocity field (Fig. 7) presents a rather uniform pattern all over the island having small values up to 1.5 mm/yr, with the exception of the extreme northern and western parts of Cephalonia, as well as Ithaca, where slightly higher values were calculated (about 2 mm/yr) that may be attributed to the longest distance from the reference point. The previous small values of standard deviation encompassing almost all the island of Cephalonia represent a ground deformation which is of an almost linear character throughout the ERS time span of 1992 to 2000.

A complete change of the velocity standard deviation of the ENVISAT data (Fig. 8) compared to the previous ERS data was resulted. A strong deviation from a linear deformation pattern is observed: The small standard deviation values (<1.5 mm/yr) are limited only in the vicinity of the reference point. At the southwestern part of the F2 zone, even though it is close to the reference point, the standard deviation was increased up to 2 mm/yr showing thus a non-linear behavior. The non-linear character of the ENVISAT velocity field becomes more profound at the Paliki Peninsula and north of F1 thrusting zone reaching the highest values. A similar pattern is also observed at Ithaca (Fig. 8). Therefore, it is evident that a discrete change in the character of the deformation field occurred sometime within the ENVISAT period between 2003 and 2008.

4.5. The acceleration field

Together with the velocity field shown above, the acceleration field of the ERS and ENVISAT data is also presented in Figs. 9 and 10, respectively. The acceleration field was obtained by fitting a second order polynomial to the time series (ts) of each PS point, that is:

$$ts = at^2 + bt + c$$

where a, b and c are the coefficients. The acceleration has the meaning of rate of change in the velocity, and it is calculated as the second order derivative of the above model versus time (t):

$$\text{Acceleration} = d^2(ts)/dt^2 = 2a.$$

Table 3
ERS and ENVISAT descending radar images.

Id	Date	Satellite	Bn[a]	Bt[days][b]
1	4/19/1992	ERS-1	0.47	−1809
2	8/22/1993	ERS-1	−0.59	−1319
3	10/31/1993	ERS-1	0.15	−1249
4	3/28/1995	ERS-1	−0.99	−736
5	5/2/1995	ERS-1	−0.71	−701
6	6/6/1995	ERS-1	−0.26	−666
7	7/11/1995	ERS-1	−0.59	−631
8	8/15/1995	ERS-1	−0.13	−596
9	8/16/1995	ERS-2	−0.18	−595
10	9/19/1995	ERS-1	−0.50	−561
11	9/20/1995	ERS-2	−0.37	−560
12	10/24/1995	ERS-1	0.33	−526
13	10/25/1995	ERS-2	0.41	−525
14	11/28/1995	ERS-1	−0.54	−491
15	1/2/1996	ERS-1	−0.03	−456
16	1/3/1996	ERS-2	−0.19	−455
17	3/12/1996	ERS-1	0.06	−386
18	3/13/1996	ERS-2	0.01	−385
19	1/22/1997	ERS-2	−0.25	−70
20	2/26/1997	ERS-2	−0.29	−35
(Master Image) 21	4/2/1997	ERS-2	0	0
22	5/7/1997	ERS-2	−0.42	35
23	8/20/1997	ERS-2	−0.09	140
24	9/24/1997	ERS-2	−0.31	175
25	12/3/1997	ERS-2	−0.10	245
26	1/7/1998	ERS-2	−0.27	280
27	3/18/1998	ERS-2	−0.23	350
28	4/7/1999	ERS-2	0.08	735
29	5/12/1999	ERS-2	0.12	770
30	6/16/1999	ERS-2	−0.73	805
31	7/21/1999	ERS-2	0.19	840
32	9/29/1999	ERS-2	0.12	910
33	11/2/1999	ERS-1	0.02	944
34	11/3/1999	ERS-2	−0.21	945
35	4/26/2000	ERS-2	0.35	1120
36	5/31/2000	ERS-2	−0.32	1155
37	8/9/2000	ERS-2	0.09	1225
38	10/18/2000	ERS-2	0	1295
39	12/27/2000	ERS-2	−0.48	1365

Id	Date	Satellite	Bn[a]	Bt[days][b]
1	6/25/2003	ENVS2-V	−0.13	−700
2	1/21/2004	ENVS2-V	−0.48	−490
3	3/31/2004	ENVS2-V	0.85	−420
4	5/05/2004	ENVS2-V	−0.79	−385
5	6/09/2004	ENVS2-V	0.33	−350
6	7/14/2004	ENVS2-V	−0.01	−315
7	8/18/2004	ENVS2-V	−0.48	−280
8	10/27/2004	ENVS2-V	0.38	−210
9	1/05/2005	ENVS2-V	0.15	−140
(Master Image) 10	5/25/2005	ENVS2-V	0	0
11	11/16/2005	ENVS2-V	0.31	175
12	3/01/2006	ENVS2-V	−0.09	280
13	6/14/2006	ENVS2-V	−0.03	385
14	7/19/2006	ENVS2-V	0.82	420
15	8/23/2006	ENVS2-V	0.58	455
16	9/27/2006	ENVS2-V	−0.65	490
17	11/01/2006	ENVS2-V	−0.47	525
18	2/14/2007	ENVS2-V	−0.18	630
19	8/08/2007	ENVS2-V	−0.1	805
20	12/26/2007	ENVS2-V	−0.31	945
21	5/11/2008	ENVS2-V	0.06	1260

[a] Bn: fraction of the critical baseline (M) Master Image: ERS = 1286.9 m, ENVISAT = 1095.8 m.
[b] Bt: days elapsed with respect to the Master Image.

The physical meaning of the acceleration field is to describe the rate of the velocity change of the PS points; therefore the sign of the velocity (positive or negative) has to also be taken into consideration. Considering PS points with positive sign of velocity (uplift), the positive acceleration is associated with *increasing* rate of uplift motion, while the negative sign of acceleration corresponds to *decreasing* rate of the uplift motion. Where a negative sign of velocity (subsidence) is observed at PS points having a positive acceleration, it corresponds to subsidence with a *decreasing* rate, while the negative acceleration indicates *increasing* rate of subsidence. Characteristic examples of PS points corresponding to these four cases of ground motion are diagrammatically shown in Fig. 11.

The acceleration field for the ERS data set is presented separately for positive and negative velocity filed (Fig. 9a, b). It can be shown that at the western and the SE part of the island where subsidence was observed (Fig. 5), that motion is characterized by a *decreasing rate* of subsidence (Fig. 9a). At the central and the northern part

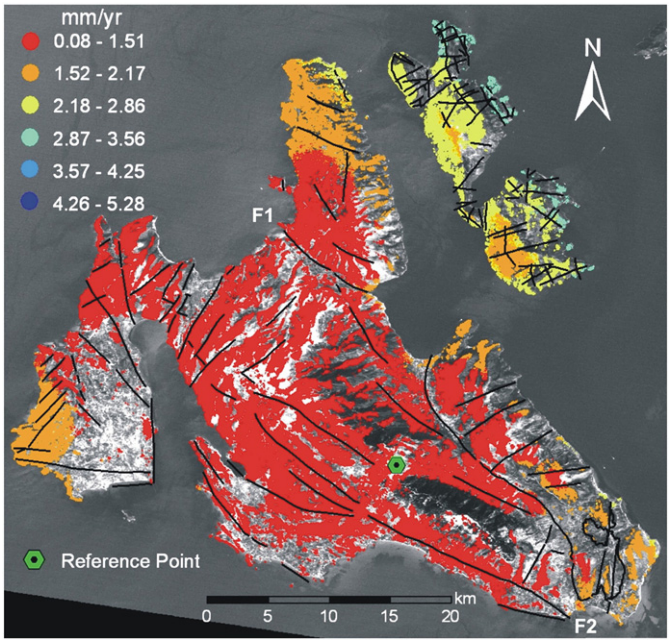

Fig. 7. Standard deviation of PSInSAR™ velocity deformation map deduced from ERS radar imaging (1992–2000).

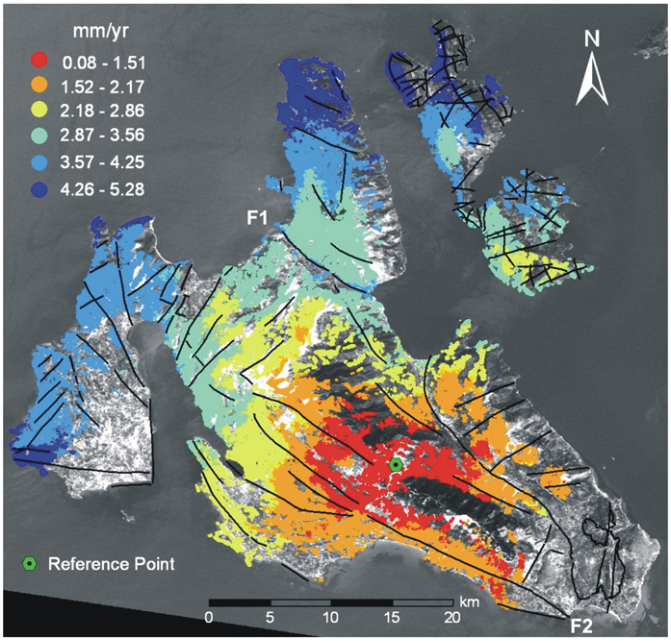

Fig. 8. Standard deviation of PSInSAR™ velocity deformation map deduced from ENVISAT radar imaging (2003–2008).

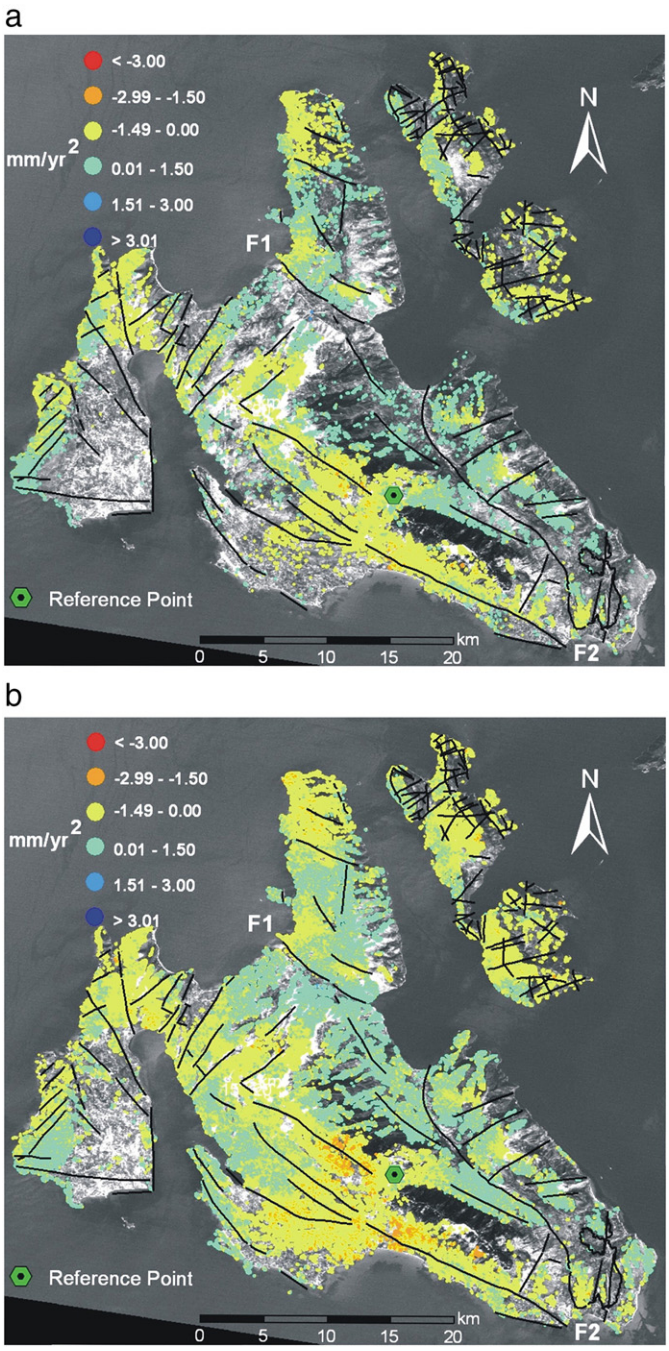

Fig. 9. Acceleration imaging for (a) negative and (b) positive PSInSAR™ velocities deduced from ERS radar imaging (1992–2000).

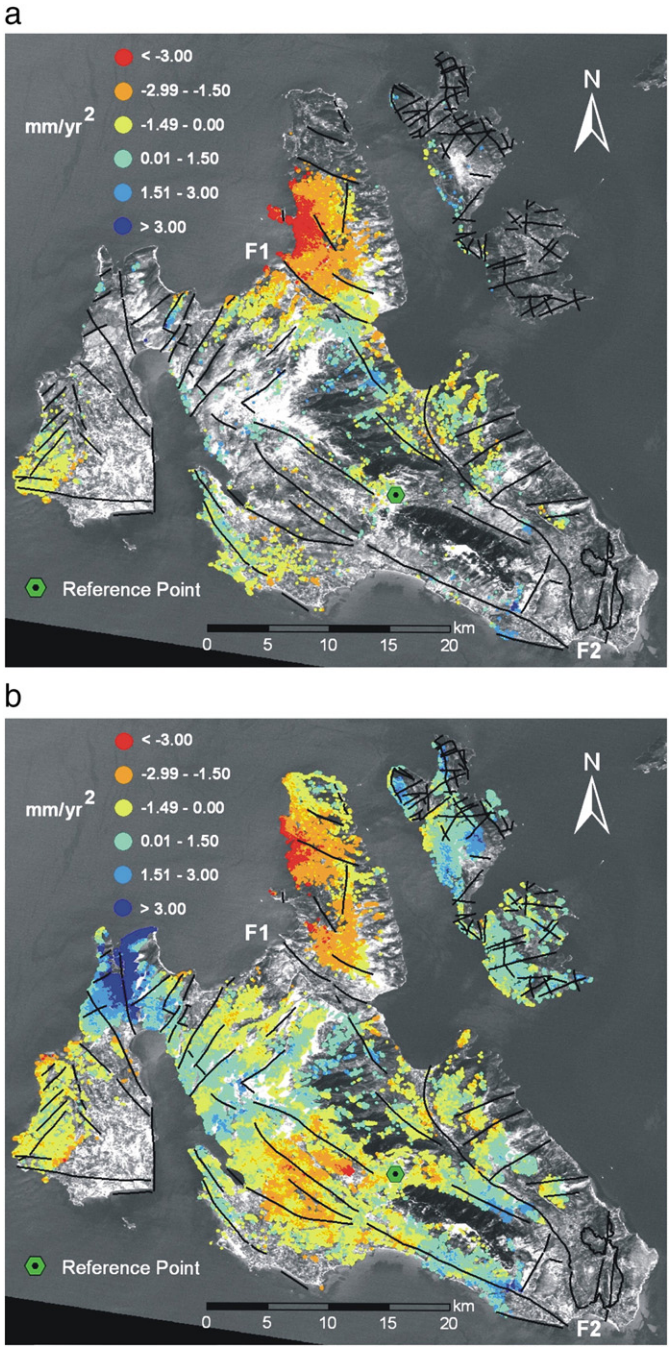

Fig. 10. Acceleration imaging for (a) negative and (b) positive PSInSAR™ velocities deduced from ENVISAT radar imaging (2003–2008).

where slight uplift (about 1 mm/yr) was observed (Fig. 5), the rate of that uplift is also decreasing (Fig. 9b).

Considering the ENVISAT data acceleration fields (Fig. 10a, b), the area where subsidence was observed is mainly noticed just north of the F1 thrust zone (Fig. 10a) with an *increasing rate* (up to −4 mm/yr^2). On the contrary, *increasing rate* of uplift was observed at the northern part of Paliki Peninsula as well as at the southeastern part of the island along the F2 thrust zone (Fig. 10b). Uplift but of a *decreasing rate* was observed at the central part of Cephalonia and the extreme western part of Paliki Peninsula (Fig. 10b).

Uplift is generally taking place in Ithaca Island (Figs. 5 and 6). However the rate of this uplift is of a decreasing character, as deduced by the ERS data (Fig. 9b). After 2003, it appears that the uplift rate *has increased* (Fig. 10b) as shown by the ENVISAT data.

5. Seismicity Pattern Analysis

The identification of seismic precursors before the occurrence of a large earthquake will be considered in this section. Several methods were proposed to identify seismic precursors like the seismic quiescence by Wyss and Habermann (1988) and the Stress Accumulation Model by Bowman and King (2001a). The most frequently used method is the accelerating seismic energy/moment release (AMR) proposed by Bufe and Varnes (1993) despite the different methodologies. This model is expressed by a simple power-law time-to-failure equation, and it is used in several implications on earthquake physics and earthquake predictability (Ben-Zion, 2008; Bowman and King, 2001b; Jaumé and Sykes, 1999; Keilis-Borok, 2002; Mignan et al., 2006; Rundle et al., 2003; Zöller and Hainzl, 2002, among many

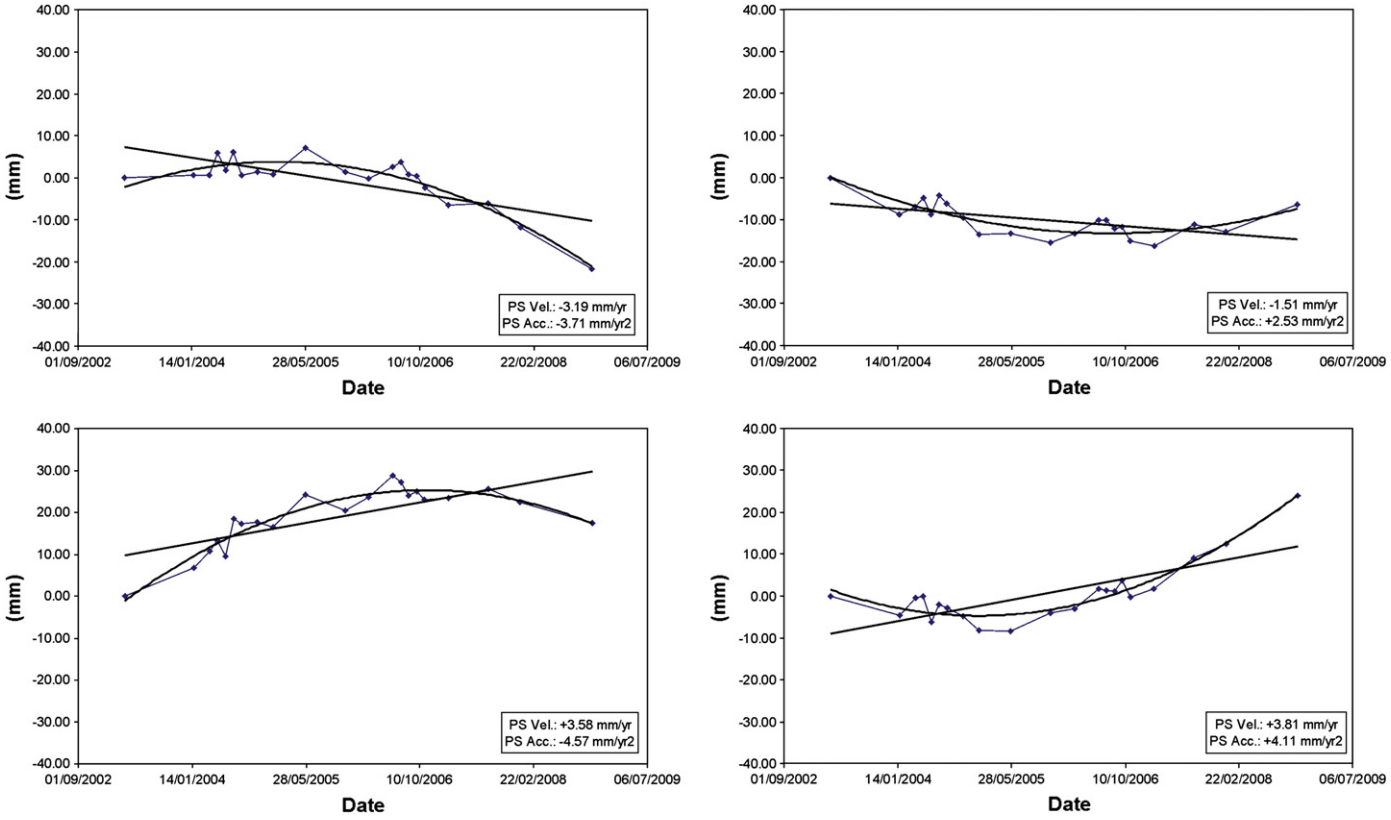

Fig. 11. Time series of selective PS points demonstrating variations with: lower diagrams: positive PSInSAR™ velocity variations (indicating uplift) with negative (left) and positive (right) acceleration. Upper diagrams: negative PSInSAR™ velocity variations (indicating subsidence) with negative (left) and positive (right) acceleration.

others). The AMR is a measure of seismicity that can be estimated from earthquake catalogs using the event magnitude to calculate the seismic moment or energy. An important characteristic of such measure is the spatio-temporal scale over which it is observed. Such a precursor that occurs during the preparation process of a large earthquake was detected in different regions in the world (Bowman et al., 1998; De Santis et al., 2010; Di Giovambattista and Tyupkin, 2004; Mignan and Di Giovambattista, 2008; Papazachos et al., 2002, 2010).

A recent work based on the decelerating and the accelerating moment release leads to the decelerating–accelerating moment release (DAMR) methodology proposed by Papadimitriou (2008). The DAMR constitutes a double seismic precursor identified in space and time before the occurrence of an earthquake. The proposed methodology was successfully applied in different regions in the world using events that occurred in the past. Additionally, the proposed methodology successfully estimates the June 2008 Andravida earthquake ($M_w = 6.4$) occurrence (Fig. 1) (Gallovič et al., 2009; Ganas et al., 2009; Konstantinou et al., 2011; Papadopoulos et al., 2010) in the Ionian region (Papadimitriou, 2008). The methodology employed in the analysis is based on four different approaches designed to discriminate and quantify spatio-temporal changes, and thus estimate the critical space and time prior to an earthquake. A brief description of this methodology is outlined in the following.

5.1. Applied methodology

The DAMR methodology was applied to identify precursory seismic patterns in space and time in the broader area of Western Greece. The selected region was considered to identify an area that can clearly be divided into two different sub-areas: the first one which is the narrow central area presents the decelerating energy release and is related to the seismogenic area, while the second one which is the broader area indicates the accelerating energy release. These seismic patterns must occur in different space and time windows. The accelerating seismic strain is based on the relation proposed by Bufe and Varnes (1993):

$$s(t) = A - \frac{B}{m}(t_c - t)^m \tag{1}$$

where $s(t)$ is a measure of seismic energy release, called the Benioff strain, t_c is the origin time of the mainshock, B is a positive constant and m is a parameter which represents the degree of accelerating (<1) or decelerating (>1) energy release. A is the value of $s(t)$ when $t = t_c$ and represents the total Benioff strain. In addition, the observed cumulative Benioff strain $\varepsilon(t)$ is defined as the sum of the square root of the observed energy release over N selected events up to time t.

The quality factor Q_t represents the temporal variation of energy release, and is calculated using the moving window technique and is defined as (Papadimitriou, 2008):

$$Q_t(t) = \frac{1}{k}\sum_{i=1}^{k} \varepsilon_i(t) \tag{2}$$

where $\varepsilon_i(t)$ is the observed Benioff strain of the ith event and k is a fixed number of selected events. The factor Q_t must fluctuate around a reference level (background level) in case of absence of large events, and must indicate a large anomaly when an earthquake is approaching. This temporal anomaly is characterized by two different time windows: the first by decelerating seismicity where the mean temporal variation of Q_t drops to a minimum level, and the second by accelerating seismicity until the occurrence of the main event. The end of this time period must asymptotically converge to the occurrence time t_c.

The identification of the critical area/time is estimated by the quality factor Q_c and as proposed by Papadimitriou (2008) is defined as:

$$Q_c\left(\vec{x},t\right) = a \cdot m \cdot c \tag{3}$$

where the constant a is an amplification factor. In the present study, no amplification is needed and a equals to unity. The parameters m, c, B and t_c (A is fixed) are calculated by the relation (1) using the least squared method. Based on the grid technique, the quality factor Q_c is calculated at each node of a predefined grid and becomes critical for values $Q_c << 1$. This method estimates the size of the critical area as well as the occurrence time t_c at each node. Thus the factor Q_c acts as an identifier, and the procedure may be considered as a pattern recognition process.

Finally the identification of the critical area is also estimated by the quality factor Q_s and is defined as (Papadimitriou, 2008):

$$Q_s\left(\vec{x},t_1,t_2\right) = \sum_{i=1}^{N(t)} \varepsilon_i\left(\vec{x}_i,t_i\right) \tag{4}$$

where $[t_1, t_2]$ is the selected time window. The selected events have epicentral distances $|\vec{x} - \vec{x}_i| \le r$, and $N(t)$ is the number of the events within the selected cylindrical volume. The factor Q_s is calculated at each node of a prefixed grid and represents the energy release of a certain geographic position. This procedure can discriminate areas of low (seismic quiescence) from those of high seismic energy release.

5.2. Data processing

Reliable catalogs of seismicity as a function of space, time and magnitude are necessary for the investigation of the evolving characteristics of seismic patterns before the occurrence of large events. In order to detect seismic precursors a seismological catalog must be characterized by independent events due to the tectonic process. A seismological catalog usually contains aftershocks and swarms that produce step-like function changes in the regional seismicity rate. The algorithm of Reasenberg (1985) is used to remove these perturbations in the present study. The used catalog included data from 1996 to 2007 (Papadimitriou et al., 2010) and was updated until June 15, 2011, using data from the Hellenic Unified Seismological Network (HUSN) operating since 2008 (http://www.geophysics.geol.uoa.gr/frame_en/netwo/nationalnet_en.html). The original catalog included 1428 events with magnitude $M > 3.5$ for the selected region $37° < \text{latitude} < 39°$ and $19° < \text{longitude} < 22°$ and the time period $\Delta T = [1996, 2011.4]$. The completeness of the catalog was subsequently evaluated based on the frequency–magnitude distribution cumulated from above and below, as it is described by Papadimitriou (2008). The final declustered catalog contained 976 events with magnitude $M > 3.5$, and presents a completeness above this magnitude.

5.3. Data analysis

The application of the same procedure was considered to investigate whether the area of western Greece is susceptible to a future large earthquake. For this reason the possibility of the occurrence of an earthquake was examined in the rectangular area $37° < \text{latitude} < 39°$ and $19° < \text{longitude} < 22°$. The identification of the candidate area is estimated by the two independent factors Q_c and Q_s, the occurrence time by the factor Q_t and the accelerating seismicity $s(t)$. The possibility of a large magnitude earthquake must be considered in case all these four methods indicate seismic precursors. The three quality factors Q_s, Q_c and Q_t as well as the accelerating seismicity $s(t)$ are calculated in the following to investigate the evolving characteristics of the seismic pattern.

5.4. Identification of critical area

The quality factor Q_s was first calculated for the time period $\Delta T = [2000, 2011.5]$. The region was divided into a grid of $0.01° \times 0.01°$ spacing, and events with focal depth $d_i \le 40$ km and magnitude $M_{min} \ge 3.6$ were selected. At each node, the factor Q_s was calculated for all events situated within the cylindrical volume of 10 km radius. The spatial distribution of Q_s (Fig. 12a) clearly indicates that an area centered at [20.50°, 37.85°], south of Cephalonia and west of Zakynthos, is characterized by low seismic activity (small circle with radius $R_1 = 30$ km). Furthermore, the surrounding area up to the larger circle with radius $R_2 = 75$ km, exhibits higher levels of energy release, and two main clusters can be recognized inside of this area: the first one located west of Cephalonia that should be attributed to a moderate event of magnitude $M_w = 5.1$ which occurred on November 16, 2003; the second one located south of Zakynthos that should rather be associated with a moderate earthquake which occurred on

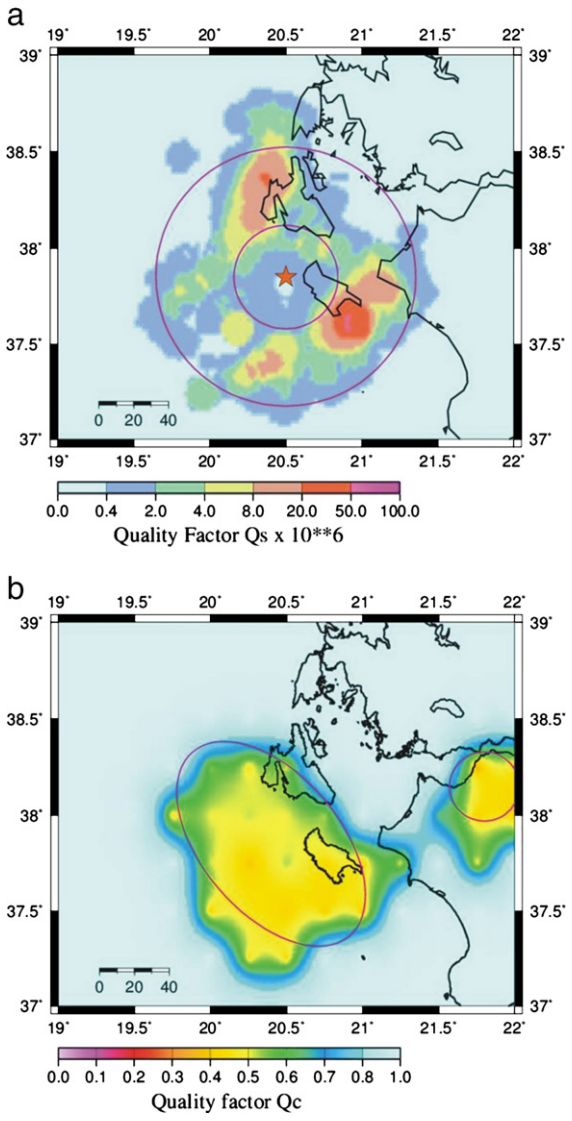

Fig. 12. (a) Spatial distribution of the quality factor Q_s for the selected region. The star indicates the center of the two circles indicating low (inside small circle) and high seismic energy release (area between the two circles). (b) Spatial distribution of the quality factor Q_c identifying the critical area for the selected region. Two areas were identified indicated by a large ellipse on the west, and a small circle NW of Peloponnese.

April 12, 2006, with magnitude $M_w = 5.7$. Both earthquakes were followed by a significant number of aftershocks. Therefore, the recognized pattern can be divided in two independent sub-areas, one characterized by low (inner circle) energy release, and the other one defined between the two circles (doughnut pattern) by high energy release.

The quality factor Q_c was secondly calculated for the time period $\Delta T = [2000, 2011.5]$. The selected region was divided into a grid of $0.25° \times 0.25°$ spacing. Considering circles with $R = 90$ km and whose centers are the nodes, the region was considered for the identification of an area in which the quality factor Q_c becomes critical. Fig. 12b shows the spatial distribution of this factor, where values of $Q_c < 0.6$ indicate the existence of a critical area. An area to the southwest of Cephalonia and to the west of Zakynthos with values $Q_c < 0.6$ is identified. The size of the area is equivalent to an elliptical area of about 80 km × 140 km and should be compared with the one revealed by Q_s.

The analysis revealed also a secondary smaller area located at the northwestern part of Peloponnese (indicated by a circle of radius $R = 20$ km). The region presents a complex tectonic setting, mainly dominated by the Hellenic Arc west of Zakynthos and by the back-arc deformation (east of the island). A similar pattern was identified by Papadimitriou (2008), where the Andravida large magnitude earthquake was located just south of this smaller area.

5.5. Identification of critical time

The temporal variation of the quality factor Q_t was calculated for the time period $\Delta T = [2000, 2011.4]$ where events with magnitude $M_{min} \geq 3.7$ and focal depth $d_i \leq 40$ km was selected. The temporal variation Q_t (Fig. 13a) has a mean value equal to 18 $J^{1/2}$. It is evident that the values of Q_t have been decreasing continuously since 2007. Considering the value Q_t on 2007.5 as the background level, the energy level reaches a minimum in 2009.3, defining the first time period $\Delta T_d = [2007.5, 2009.3]$. Following this period, an increase of the energy level is observed defining a second time period $\Delta T_a = [2009.4, 2010.8]$. At this time, an abrupt increase is observed defining the third time period $\Delta T_i = [2010.9, 2011.5]$. The temporal analysis clearly identified the existence of a double precursor indicating two independent decelerating–accelerating time periods. At the end of this period (extrapolating asymptotically toward the background level), the occurrence time $T_c = 2011.8$ may be estimated and marked by a star (Fig. 13a).

In the previous part of the curve (Fig. 13a) where the decelerating and accelerating patterns are shown, the two seismic sequences that occurred (the first one on 2003.9 west of Cephalonia, and the second one on 2006.3 south of Zakynthos) have successfully been predicted (these events were also mentioned in a previous section). The occurrence time of these events is indicated by bars at the top of Fig. 13a.

Finally, the Benioff strain $s(t)$ versus time was calculated, and is presented in Fig. 13b, assuming a magnitude $M_w = 6.5$. This variation is approximately linear for the time period 2008–2010, thus corresponding to the null hypothesis that the seismicity rate is constant. After this period, acceleration is evident and this variation becomes non-linear. The calculated degree of acceleration is $m = 0.52$, and the estimated occurrence time $t_c = 2011.7$ (point with the red open circle). This m value is an indicator of high ($m < 0.4$) or low ($m > 0.6$) possibility on the accuracy of the occurrence of a seismic event (Papadimitriou, 2008). The resulting calculated value of m ($= 0.52$) is considered as a moderate value introducing an error estimate of about ±1 year. It is evident therefore that an accelerating seismic crustal deformation has been taking place in the area since 2010. This estimated time t_c is similar to the one calculated by the temporal variation T_c indicating the possibility of a large magnitude seismic event at about the end of 2011. Nevertheless, the latter time estimates deduced by the modelling should be critically considered and thoughtfully evaluated as to the (i) moderate resulting value of m, (ii) the degree of the updated earthquake catalog incorporating the latest data set and (iii) the inherent limitations in the applied modelling procedure.

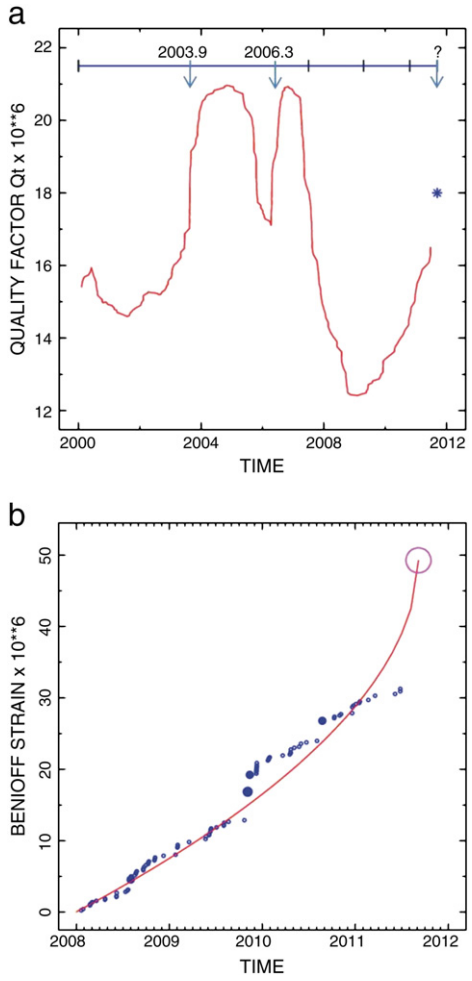

Fig. 13. (a) Temporal variation of the quality factor Q_t. The star represents the occurrence time of a possible future seismic event. The horizontal line marked by vertical bars indicates the time period of background seismicity, ΔT_d, ΔT_a, and ΔT_i. (b) Theoretical (solid line) and observed (circles) cumulative Benioff strain variation $s(t)$. Red open circle represents the occurrence time of a probable future seismic event.

6. Discussion — conclusions

It is important to point out not only the aspect of the common ground control point that was chosen as reference point for the GPS network and the PS Interferometric analysis (No. 06), but also the knowledge of its motion in time and space with respect to ITRF2000. This is a point of a consistent behavior and proven stability in the vertical component since at least 2001 (Fig. 3), and therefore provides a confident and direct comparison between the observed DGPS results (2001–2010) and the produced PS image, at least for the ENVISAT data (2003–2008).

PS Interferometry results from Cephalonia illustrate a continuous and consistent pattern of vertical deformation from 1992 to 2000. This is inferred by the small values of standard deviation prevailing almost in the whole island of Cephalonia (Fig. 7) that indicates a ground deformation which is of an almost linear character throughout the ERS time span of 1992 to 2000.

The period though after 2003 presents a different deformation picture consisting of two main characteristics: (i) the sign of the vertical

ground motion has mostly reversed to uplift (Fig. 6), and (ii) a deviation from the linear deformation model is strongly noticed (Fig. 8). These aspects were particularly pronounced at Paliki Peninsula, and along a wide zone extending mainly along the southern parts the island, from NW to SE, on both sides of the F2 thrusting zone. The sign change in the ground motion and the non-linear behavior of deformation in those areas was also noted on the DGPS results after the remeasurement of the network in 2003 (Lagios et al., 2007), marking a dramatic change in the tectonic behavior of the Cephalonia Island.

The uplift in Paliki Peninsula (about 70 mm) reached the highest observed amplitudes (Fig. 4b), but it was of a decreasing rate (Fig. 10b), consistent with the DGPS observations that showed a decline after 2007. On the contrary, along and across the NW–SE F2 trending zone the observed uplift was of an increasing rate character (Fig. 10b). Prior to 2003, the ground deformation in the latter area was consistent with the known and expected neotectonic movements of the area indicating a slight subsidence. After 2003, the high magnitudes of uplift may be indicative of a major regional crustal deformation process of a bulging character that could be taking place in the broader region, in the marine area SW and south of Cephalonia, something that is now consistent with the results of the seismicity analysis (Fig. 13). At an attempt to interpret that change of the ground deformation pattern, the concept of dilatancy was envisaged for this phenomenon when it was first recognized based only on the GPS data (Lagios et al., 2007). The comparison between ERS and ENVISAT PS products, however, provides now an additional qualitative and quantitative supporting image verifying the uplifting of the area, first depicted by the limited point coverage of the DGPS study in 2006 (Lagios et al., 2007).

The identification of a seismically critical area that may generate a large seismic event to the south and southwest of Cephalonia (Fig. 12a, b) was deduced by two independent seismic methodologies based on (i) the observed energy release (Fig. 12a), and (ii) the modelling of the observed seismic accelerating strain (Fig. 12b). The identified major seismically critical area (Fig. 12b) marginally encompasses the regions along the western and southern parts of the island, where the maximum uplift rates were observed from both DGPS and PS analysis, and may geodynamically contribute to the process of the bulging on land. Another critical area of smaller horizontal extent is also noticed at the northwestern part of Peloponnese (Fig. 12b). This area seems to be extended NNE of the Andravida epicenter earthquake reaching the coast of the Patras Gulf.

On the basis of the accelerating seismicity pattern (Fig. 13b), the occurrence time of a large magnitude event was determined at about the end of 2011. A very close critical occurrence time to the previous one was also deduced by the decelerating–accelerating seismicity time period analysis (Fig. 13a).

If the dilatancy hypothesis (adopted to interpret the uplifted regions in Cephalonia) is valid, applying the formulae by Rikitake (1975, 1987), and on the basis of the areal extent of the observed crustal deformation area (≥50 km) deduced by DGPS and PS results, a preparatory period of at least 5.3 ± 0.1 years is calculated for a reference magnitude $M = 7$ seismic event, noting that an upper limit of a magnitude $M = 7.2$ is estimated for a deformation area of 50 km areal extent. If the magnitude event (M) is in its upper limit ($M = 7.2$) value, the preparatory period results in 6.6 ± 0.2 years. Nevertheless, it should be noted that these estimated values of the preparatory period should be considered as only indicative (Rikitake, 1987), since there were not many available earthquakes of magnitude around seven (7) for the estimation of the empirical formula (preparatory period versus magnitude event), and therefore larger error estimates are inevitably inherent.

If a large magnitude seismic event (M) takes place in the limit $7.0 \leq M \leq 7.2$, the indicative precursory estimated value of 5.3 to 6.6 years should in any case be considered after mid-2005, when the uplifting phenomenon was determined to have basically started on the western and southern parts of Cephalonia. The period of mid-2005 (±6 months) was concluded by examining the time series of several PS ENVISAT points at the western and along the southern parts of Cephalonia. Two representative diagrams of PS time series from such points in those areas, especially from Paliki Peninsula and Sissia area (No. 22 GPS station, Fig. 1), are shown in Fig. 14, where it can be seen that the uplift starts taking place at about mid-2005.

Concluding, a fairly good agreement in the determination of the critical area for a probable strong future seismic event was deduced by independent methodologies, namely the evaluation of the ground deformation (DGPS and PS Interferometry) and the Seismicity Pattern Analysis of the broader area. This area mainly extends offshore SW of Cephalonia including the southern and western parts of the island. As to the critical time estimations of these different methodologies, which lead to a similar time-window, these independently produced results should be considered with caution; mainly due to their indicative character already mentioned above, as well as to the probably inherent unknown tectonic characteristics and parameters involved in that very complex area of study. These objectively uncertain issues might be able to influence and possibly change the evolution of the seismicity pattern and its associated resulting (non-unique inversion) modelling attempts that were produced by the available seismicity data presented in this paper up to mid-June 2011. Note that the DGPS observations were up to early 2010, and the availability for the ENVISAT radar imaging for the compilation of the PSI image was up to 2008 (Table 3). The lack of updating in the former data, combined with possible seismicity rate change, may have such kind of characteristics that could possibly be able to strongly influence not only the deduced critical area and/or the critical time estimations, but also even the possibility on the occurrence of a forthcoming strong seismic event.

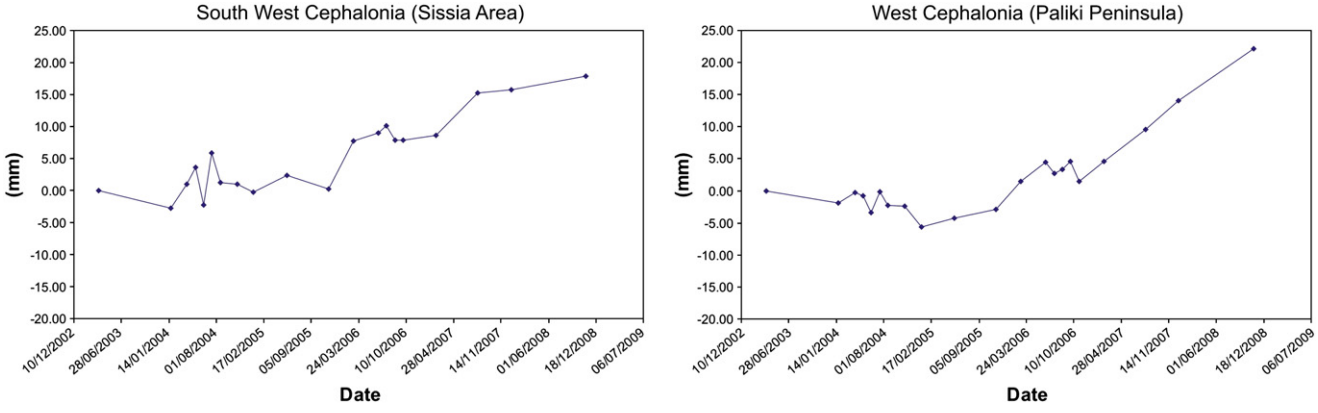

Fig. 14. Time series of selective PS points depicting the commencement of uplift at Sissia area and Paliki Peninsula.

Acknowledgments

The PS Interferometric analysis was performed within the framework of TERRAFIRMA Stage-3 Project (www.terrafirma.eu.com). Part of the GPS work was financed by *KAPODISTRIAS* (NKUA), the GSRT and EPPO (Athens, Greece). We would like to thank Dr. Sp. Vassilopoulou (NKUA) for her GIS contribution and Dr. Brian Damiata (UCLA) for establishing the GPS stations in Ithaca. GMT software (http://gmt.soest.hawaii.edu/) was used to generate some figures.

References

Anzidei, M., Baldi, P., Casula, G., Crespi, M., Riguzzi, F., 1996. Repeated GPS surveys across the Ionian Sea: evidence of crustal deformations. Geophysical Journal International 127, 257–267.

Aubouin, J., Dercourt, J., 1962. Zone Preapoulien, Zone Ionienne et Zone de Gravrovo en Pelloponnese occidentale. Bulletin de la Societe Geologique de France 4, 785–794.

Ben-Zion, Y., 2008. Collective behavior of earthquakes and fault: continuum–discrete transitions, progressive evolutionary changes, and different dynamic regimes. Reviews of Geophysics 46, RG4006. doi:10.1029/2008RG000260.

Bowman, D.D., King, G.C.P., 2001a. Stress transfer and seismicity changes before large earthquakes. Comptes Rendus de l' Academie des Sciences 333, 591–599.

Bowman, D.D., King, G.C.P., 2001b. Accelerating seismicity and stress accumulation before large earthquakes. Geophysical Research Letters 28, 4039–4042.

Bowman, D.D., Ouillon, G., Sammis, C.G., Sornette, A., Sornette, D., 1998. An observational test of the critical earthquake concept. Journal of Geophysical Research 103 (24), 359–372.

Bufe, C.G., Varnes, D.J., 1993. Predictive modelling of the seismic cycle of the Great San Francisco Bay Region. Journal of Geophysical Research 98, 9871–9883.

Dach, R., Hugentobler, U., Fridez, P., Meindl, M., 2007. Bernese GPS Software Version 5.0. Astronomical Institute, University of Bern, Bern.

De Santis, A., Cianchini, G., Qamili, E., Frepoli, A., 2010. The 2009 L' Aquila (Central Italy) seismic sequence as a chaotic process. Tectonophysics 496, 44–52.

Di Giovambattista, R., Tyupkin, Y.S., 2004. Seismicity patterns before the M = 5.8 2002, Palermo (Italy) earthquake: seismic quiescence and accelerating seismicity. Tectonophysics 384, 243–255.

Ferretti, A., Prati, C., Rocca, F., 2000. Analysis of Permanent Scatterers in SAR interferometry. International Geoscience & Remote Sensing Symposium (IGARSS) 2, 761–763.

Ferretti, A., Prati, C., Rocca, F., 2001. Permanent scatterers in SAR interferometry. IEEE Transactions on Geoscience and Remote Sensing 39 (1), 8–20.

Gallovič, F., Zahradník, J., Křížová, D., Plicka, V., Sokos, E., Serpetsidaki, A., Tselentis, G.-A., 2009. From earthquake centroid to spatial–temporal rupture evolution: Mw 6.3 Movri Mountain earthquake, June 8, 2008, Greece. Geophysical Research Letters 36, L21310.

Ganas, A., Serpelloni, E., Drakatos, G., Kolligri, M., Adamis, I., Tsimi, Ch., Batsi, E., 2009. The Mw 6.4 SW Achaia (Western Greece) Earthquake of 8 June 2008: seismological, field, GPS observations, and stress modelling. Journal of Earthquake Engineering 13, 8,1101–8,1124.

Heleno, S.I.N., Oliveira, L.G.S., Henriques, M.J., Falcão, A.P., Lima, J.N.P., Cooksley, G., Ferretti, A., Fonseca, A.M., Lobo-Ferreira, J.P., Fonseca, J.F.B.D., 2011. Persistent Scatterers Interferometry detects and measures ground subsidence in Lisbon. Remote Sensing of Environment 115 (8), 2152–2167.

Hollenstein, Ch., Geiger, A., Kahle, H.-G., Veis, G., 2006. CGPS time-series and trajectories of crustal motion along the West Hellenic Arc. Geophysical Journal International 164 (1), 182–191.

Hollenstein, Ch., Müller, M.D., Geiger, A., Kahle, H.-G., 2008. Crustal motion and deformation in Greece from a decade of GPS measurements 1993–2003. Tectonophysics 449, 17–40.

http://www.epncb.oma.be/.

http://www.geophysics.geol.uoa.gr/frame_en/netwo/nationalnet_en.html.

Jaumé, S.C., Sykes, L.R., 1999. Evolving towards a critical point: a review of accelerating seismic moment/energy release rate prior to large and great earthquakes. Pure and Applied Geophysics 155, 279–306.

Kamberis, E., Marnelis, F., Loucoyannakis, M., Maltezou, F., Hirn, A., Streamers Group, 1996. Structure and deformation of the External Hellenides based on seismic data from offshore Western Greece. In: Wessely, G., Liebl, W. (Eds.), Oil and Gas in Alpidic Thrustbelts and Basins of Central and Eastern Europe: EAGE Special Publication, No. 5, pp. 207–214.

Karakostas, V.G., Papadimitriou, E.E., Papazachos, C.B., 2004. Properties of the 2003 Lefkada, Ionian Islands, Greece, earthquake seismic sequence and seismicity triggering. Bulletin of the Seismological Society of America 94 (5), 1976–1981.

Keilis-Borok, V.I., 2002. Earthquake prediction: state-of-the-art and emerging possibilities. Annual Review of Earth and Planetary Sciences 30, 1–33.

Konstantinou, K.I., Evangelidis, C.P., Melis, N.S., 2011. The 8 June 2008 Mw 6.4 earthquake in Northwest Peloponnese, Western Greece: a case of fault reactivation in an overpressured lower crust? Bulletin of the Seismological Society of America 101 (1), 438–445. doi:10.1785/0120100074.

Lagios, E., Sakkas, V., Papadimitriou, P., Damiata, B.N., Parcharidis, I., Chousianitis, K., Vassilopoulou, S., 2007. Crustal deformation in the Central Ionian Islands (Greece): results from DGPS and DInSAR analyses (1995–2006). Tectonophysics 444, 119–145.

Le Pichon, X., Chamot-Rooke, N., Lallemant, S., Noomen, R., Veis, G., 1995. Geodetic determination of the kinematics of Central Greece with respect to Europe: implications for Eastern Mediterranean tectonics. Journal of Geophysical Research 100 (12), 675–690.

Lekkas, E., Danamos, G., Maurikas, G., 2001. Geological structure and evolution of Cefallonia and Ithaki Islands. Bulletin of the Geological Society of Greece XXXIV/1, 11–17.

Louvari, E., Kiratzi, A., Papazachos, B.C., 1999. The Cephalonia Transform Fault and its extension to western Lefkada Island (Greece). Tectonophysics 308, 223–236.

Mercier, J., Bousquet, B., Delibasis, N., Drakopoulos, J., 1972. Deformations en compression dans le Quaternaire des rivages Ioniens. (Cephalonie, Greece), Academie des Science, ceance du 30 Octobre, Paris.

Mignan, A., Di Giovambattista, R., 2008. Relationship between accelerating seismicity and quiescence, two precursors to large earthquakes. Geophysical Research Letters 35, L15306. doi:10.1029/2008GL035024.

Mignan, A., Bowman, D.D., King, G.C.P., 2006. An observational test of the origin of accelerating moment release before large earthquakes. Journal of Geophysical Research 111, B11304. doi:10.1029/2006JB004374.

Niell, A.E., 1996. Global mapping functions for the atmosphere delay at radio wavelengths. Journal of Geophysical Research 101 (B2), 3227–3246.

Papadimitriou, P., 2008. Identification of seismic precursors before large earthquakes: decelerating and accelerating seismic patterns. Journal of Geophysical Research 113, B04306. doi:10.1029/2007JB005112.

Papadimitriou, P., Kaviris, G., Makropoulos, K., 2006. The Mw = 6.3 2003 Lefkada Earthquake (Greece) and induced transfer changes. Tectonophysics 423, 73–82.

Papadimitriou, P., Kaviris, G., Karakonstantis, A., Makropoulos, K., 2010. The Cornet seismological network: 10 years of operation, recorded seismicity and significant applications. Hellenic Journal of Geosciences 45, 193–208.

Papadopoulos, G.A., Karastathis, V., Kontoes, C., Charalampakis, M., Fokaefs, A., Papoutsis, I., 2010. Crustal deformation associated with east Mediterranean strike–slip earthquakes: the 8 June 2008 Movri (NW Peloponnese), Greece, earthquake (Mw6.4). Tectonophysics 492, 201–212.

Papazachos, C.B., Karakaisis, G.F., Savvaidis, A.S., Papazachos, B.C., 2002. Accelerating seismic crustal deformation in the southern Aegean area. Bulletin of the Seismological Society of America 92, 570–580.

Papazachos, B.C., Karakaisis, G.F., Scordilis, E.M., Papazachos, C.B., Panagiotopoulos, D.G., 2010. Present patterns of decelerating–accelerating seismic strain in South Japan. Journal of Seismology 14, 273–288.

Parcharidis, I., Foumelis, M., Kourkouli, P., Wegmuller, U., 2009. Persistent Scatterers InSAR to detect ground deformation over Rio-Antirio area (Western Greece) for the period 1992–2000. Journal of Applied Geophysics 68 (3), 348–355.

Reasenberg, P.A., 1985. Second-order moment of central California seismicity, 1969–1982. Journal of Geophysical Research 90, 5479–5495. doi:10.1029/JB090iB07p05479.

Reilinger, R., McClusky, S., Paradissis, D., Ergintav, S., Vernant, P., 2010. Geodetic constraints on the tectonic evolution of the Aegean region and strain accumulation along the Hellenic subduction zone. Tectonophysics 488 (1–4), 22–30.

Rikitake, T., 1975. Dilatancy model and empirical formulas for an earthquake area. Pure and Applied Geophysics 113, 141–147.

Rikitake, T., 1987. Earthquake precursors in Japan: precursor time and detectability. Tectonophysics 136, 265–282.

Rundle, J.B., Turcotte, D.L., Shcherbakov, R., Klein, W., Sammis, C., 2003. Statistical physics approach to understanding the multiscale dynamics of earthquake fault systems. Reviews of Geophysics 41. doi:10.1029/2003RG000135.

Sachpazi, M., Hirn, A., Clement, C., Haslinger, F., Laigle, M., Kissling, E., Charvis, P., Hello, Y., Lepine, J.-C., Sapin, M., Ansorge, J., 2000. Western Hellenic subduction and Cephalonia Transform: local earthquakes and plate transport and strain. Tectonophysics 319, 301–319.

Underhill, J.R., 1989. Late Cenozoic deformation of the Hellenide foreland, western Greece. Bulletin Geological Society of America 101, 613–634.

Vassilakis, E., Royden, L., Papanikolaou, D., 2011. Kinematic links between subduction along the Hellenic trench and extension in the Gulf of Corinth, Greece: a multidisciplinary analysis. Earth and Planetary Science Letters 303, 108–120. doi:10.1016/j.epsl.2010.12.054.

Vlachou, K., Sakkas, V., Papadimitriou, P., Lagios, E., 2011. Crustal deformation studies in the seismically active area of Patras Gulf (Greece). 2011 IEEE Int. Geosci. Remote Sens. Symp. (IGARSS). doi:10.1109/IGARSS.2011.6050082.

Wyss, M., Habermann, R.E., 1988. Precursory seismic quiescence. Pure and Applied Geophysics 126, 319–332.

Zahradník, J., Serpetsidaki, A., Sokos, E., Tselentis, G.-A., 2005. Iterative deconvolution of regional waveforms and a double-event interpretation of the 2003 Lefkada earthquake, Greece. Bulletin of the Seismological Society of America 95 (1), 159–172.

Zöller, G., Hainzl, S., 2002. A systematic spatiotemporal test of the critical point hypothesis for large earthquakes. Geophysical Research Letters 29. doi:10.1029/2002GL014856.